Nonlocal hyper-Rayleigh scattering from liquid nitrobenzene

David P. Shelton[a)]
Department of Physics and Astronomy, University of Nevada, Las Vegas, Nevada 89154-4002, USA

(Received 3 November 2009; accepted 18 March 2010; published online 20 April 2010)

Hyper-Rayleigh scattering (HRS) from liquid nitrobenzene was measured for several combinations of linear polarized incident and scattered light, for a range of scattering angles near 90°. The observations show that the HRS intensity is dominated by the polar transverse collective mode contribution, and support a model where the long range dipole-dipole orientation correlations in a polar liquid result in coherent HRS from $\beta^{(1)}$, the vector part of the molecular first hyperpolarizability β, whereas HRS from the octupolar part $\beta^{(3)}$ remains local and incoherent. © *2010 American Institute of Physics*. [doi:10.1063/1.3385893]

I. INTRODUCTION

Hyper-Rayleigh scattering (HRS) in liquids is second harmonic light scattering mediated by the molecular first hyperpolarizability tensor β.[1–4] The strong electric field of the incident laser light at frequency ν induces small dipoles oscillating at frequency 2ν in the noncentrosymmetric molecules in the liquid. The phase and amplitude of the induced dipole varies with the orientation of the molecule, so that the fields radiated from the oscillating molecular dipoles add incoherently in the case of randomly oriented molecules. In that case, the observed HRS intensity for a molecular liquid is related to the isotropic orientation averaged squared tensor $\langle\beta^2\rangle$, and information about the relative size of the tensor components of β may be inferred from measurements of the dependence of the HRS intensity on the polarization of the incident and scattered light.[1–8]

However, the observed polarization dependence of HRS from several polar liquids is inconsistent with the usual assumption of random molecular orientation.[9–11] Such HRS measurements are most often made in the 90° scattering geometry with linearly polarized incident and scattered light selected. Figure 1 shows the scattering geometry. The four common experimental configurations with incident and scattered light polarized either perpendicular or parallel to the horizontal scattering plane are denoted VV, HV, VH, and HH, where V denotes vertical polarization, H denotes horizontal polarization, and the first and second letters refer to the incident and scattered light, respectively. The macroscopic isotropy of a liquid requires that HRS intensity $I_{\mathrm{HV}}=I_{\mathrm{VH}}$ in the case that both the scattering units and the range of their orientation correlations are small compared with the light wavelength. The violation of this equality indicates contributions from collective modes.[9–13]

A collective mode which is longitudinally polarized with respect to the scattering vector $\Delta\mathbf{k}=2\mathbf{k}_{\nu}-\mathbf{k}_{2\nu}$ has been observed in HRS experiments, due to the long range orientation correlations of polar molecules induced by the electric field of dissolved ions in the liquid.[14,15] The HRS spectrum for this mode is extremely narrow with $I_{\mathrm{HV}}/I_{\mathrm{VH}}=0$. This contribution to the HRS spectrum can be suppressed by deionizing the liquid, but it may have confounded some of the measurements made before its origin was determined.[9] The polarization signature for HRS from a transverse polar collective mode is $I_{\mathrm{HV}}/I_{\mathrm{VH}}=2$, so a contribution from a transverse collective mode is indicated by $I_{\mathrm{HV}}>I_{\mathrm{VH}}$ observed for some polar liquids.[9–11] One such liquid is nitrobenzene, and the present experiment improves and extends previous work studying HRS from nitrobenzene.[9,11] The aim of the present work is to dissect the local mode and the longitudinal and transverse collective mode contributions to HRS from liquid nitrobenzene.

II. THEORY

The theory for HRS from independent randomly oriented molecules is well established. HRS measurements can in principle determine up to six invariants for the β tensor, although this may require use of elliptical polarization and a scattering angle other than 90°.[1–4] With the restriction to just V and H linear polarizations only two invariants can be determined, and all ratios of the HRS intensities I_{VV}, I_{HV}, I_{VH}, and I_{HH} can be expressed in terms of one parameter $P^2=\langle\beta^2_{ZZZ}\rangle/\langle\beta^2_{XZZ}\rangle$, where $\langle\beta^2_{ZZZ}\rangle$ and $\langle\beta^2_{XZZ}\rangle$ are squared lab-frame components of β averaged over all molecular orientations. The number of independent β tensor elements depends on the molecular symmetry, and for molecules with C_{2v} symmetry such as nitrobenzene there are five nonzero independent β components, which reduces to three in the case that Kleinman (full permutation) symmetry holds.[1,8] The parameter P^2 can be expressed in terms of the components of β in the molecular frame: β_{zzz}, β_{zyy}, β_{zxx}, β_{yyz}, and β_{xxz}, where yz is the molecular plane and z is the twofold axis (the permanent dipole also lies along z).[1,2] For an isolated nitrobenzene molecule one obtains $P^2=3.60$ from the *ab initio* calculated static electronic β components $\beta_{zzz}=-193.6$, $\beta_{zyy}=4.7$, and $\beta_{zxx}=27.4$ (atomic units; permanent dipole $\mu_z<0$).[16] An alternative representation of the β tensor is the direct sum of irreducible spherical tensors. In the case that Kleinman symmetry holds the sum is $\beta=\beta^{(1)}\oplus\beta^{(3)}$, with $P^2=9$ for $\beta^{(1)}$ and $P^2=3/2$ for $\beta^{(3)}$.[2,4] Based on the *ab initio* calculated β components for nitrobenzene the octupolar term $\beta^{(3)}$ contributes

[a)]Electronic mail: shelton@physics.unlv.edu.

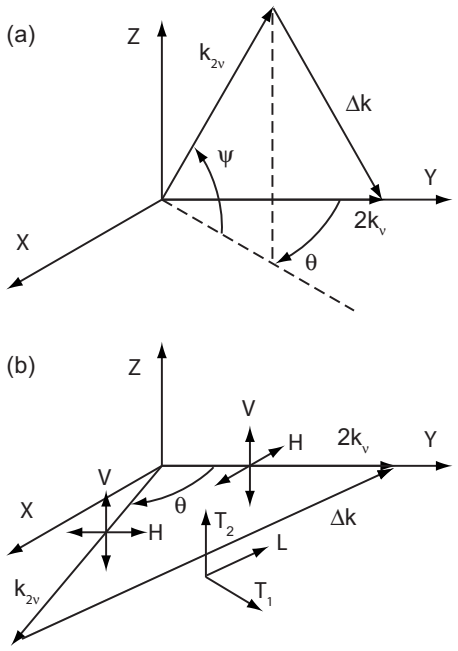

FIG. 1. Incident and scattered wavevectors, $\mathbf{k}_{\nu}$ and $\mathbf{k}_{2\nu}$, are shown for (a) scattering above the *XY* plane and (b) scattering in the *XY* plane near $\theta=90°$. For scattering in the *XY* plane the V or H linear polarization vectors are parallel or perpendicular to **Z**, respectively. For scattering out of the *XY* plane, the H polarized component of the scattered wave is still perpendicular to **Z**, while the V polarized component is perpendicular to $\mathbf{k}_{2\nu}$ in the plane spanned by **Z** and $\mathbf{k}_{2\nu}$. Longitudinal (*L*) and transverse (T_1,T_2) directions are defined with respect to the scattering vector $\Delta\mathbf{k}$, as shown in (b).

30% of I_{VV} and 72% of I_{HV}, with the vector term $\beta^{(1)}$ contributing the remainder.

The above calculation is correct for an isolated molecule, but the molecules in a liquid are not isolated, and the intermolecular interactions distort and correlate the molecules. The effect of the fluctuating local electric field due to the molecular dipoles has been included in a recent molecular dynamics simulation for HRS from liquid nitrobenzene, giving P^2 near the single molecule result.[16] Additional HRS contributions will result from the intense short range field of the higher permanent molecular multipole moments acting on neighboring molecules.[17] All these HRS contributions are local in the sense that the range of the correlations is at most a few molecular diameters, HRS from the different interactions adds incoherently, and the isotropic average HRS from any small region has angular and polarization dependence with the same functional form as that for an isolated molecule. Angular and polarization dependence different from that due to the dipole hyperpolarizabilities considered above results from the quadrupole hyperpolarizability of the molecules.[18] Quadrupolar HRS is due to two terms: the induced molecular quadrupole quadratic in the laser field (qee), and the induced molecular dipole proportional to the product of the laser field and the laser field gradient (eeq). Theoretical expressions for HRS from each of these two terms for any molecular symmetry have been derived, but the values of the quadrupolar hyperpolarizability tensor components needed to evaluate these expressions are usually unknown.[18] Other contributions at this order are due to the induced magnetic dipole quadratic in the laser electric field (mee), and the electric dipole bilinear in the laser electric and magnetic fields (eem).[19]

The calculation for HRS from polar collective modes of an isotropic liquid is based on the ansatz that the induced dipole is of the form $\mu_J^{(2\nu)}=\chi_{JKLM}E_K^{(\nu)}E_L^{(\nu)}Q_M$, where χ_{JKLM} is an isotropic tensor and Q_M is the amplitude vector for the polar collective mode.[12] The isotropic tensor χ_{JKLM} has just two independent nonzero components related by $R=\chi_{ZZZZ}/\chi_{XZZX}$ ($R=3$ in the case that Kleinman symmetry applies), and the collective modes of interest have wavevector equal to the scattering wavevector $\Delta\mathbf{k}$ and are polarized either longitudinal or transverse to $\Delta\mathbf{k}$. This construct represents a long range orientation correlation of the polar molecules in the liquid, and its form determines the angular and polarization dependence of HRS from the collective mode.[12]

Summing the HRS intensities from the randomly oriented molecules and from the collective modes gives the expressions[12]

$$I_{VV}=A_0P^2+A_TR^2, \tag{1}$$

$$I_{HV}=A_0+A_T, \tag{2}$$

$$I_{VH}=A_0+A_T\sin^2(\theta/2)+A_L\cos^2(\theta/2), \tag{3}$$

$$\begin{aligned} I_{HH}=&A_0[\sin^2\theta+P^2\cos^2\theta]\\ &+A_T[1-(R-1)\cos\theta]^2\sin^2(\theta/2)\\ &+A_L[1+(R-1)\cos\theta]^2\cos^2(\theta/2), \end{aligned} \tag{4}$$

where θ is the scattering angle in the horizontal plane, and A_0, A_T, and A_L are intensity coefficients for HRS due to local, transverse, and longitudinal modes, respectively. Expressions for HRS scattering at angles out of the horizontal plane may be similarly constructed using the results given in Ref. 12 (the Appendix gives corrected results for the transverse modes). In the case that $A_T=A_L$ the form of Eqs. (1)–(4) is just the same as for pure local mode HRS, but otherwise polar collective modes have the observable effect that $I_{HV}\neq I_{VH}$. Measurements at $\theta=90°$ are insufficient to determine all the parameters in Eqs. (1)–(4), but additional information is available from measurements over a range of angles near 90°, as can be seen from the following relations:

$$R=\frac{1}{2}+\frac{1}{2}\left[\frac{\partial I_{HH}}{\partial\theta}\Big/\frac{\partial I_{VH}}{\partial\theta}\right]_{\theta=90°}, \tag{5}$$

$$A_T-A_L=2\left[\frac{\partial I_{VH}}{\partial\theta}\right]_{\theta=90°}. \tag{6}$$

Four parameters P^2, R, A_0/A_T, and A_L/A_T are sufficient to specify the HRS contributions of the local and collective modes. Since HRS intensity ratio measurements are more accurate than HRS intensity measurements, the parameters will be determined by fitting expressions for the HRS intensity ratios I_{VV}/I_{HV}, I_{HV}/I_{VH}, and I_{HH}/I_{VH} constructed using Eqs. (1)–(4) to the corresponding experimental measurements.

III. EXPERIMENT

The HRS experimental apparatus and methods are similar to those previously described.[14,15] Figure 2 shows the apparatus. Linearly polarized pulses from an injection-seeded single-longitudinal-mode Nd:YAG (yttrium aluminum garnet) laser (operating at $\lambda=1064$ nm, 4.3 kHz repetition rate, 100 ns pulse duration) are focused into the liquid sample contained in a 1 cm fused silica spectroscopic cuvette. Light scattered near the 90° scattering angle is collected and collimated by a lens, analyzed by a polarizing beam splitter, focused by another lens into an optical fiber, and fiber coupled to spectral filters and the photon counting detector. The sample temperature was $T=25.0$ °C for all measurements, and the laser beam (LB) average power in the sample was typically 1 W. The sample was deuterated nitrobenzene ($C_6D_5NO_2$, Isotec, 99.5 at. % D) to minimize thermal lens effects due to absorption of the laser beam.

Several modifications were made to better define and control the scattering geometry and more accurately measure the ratios of HRS intensities for various combinations of incident and scattered light polarization (polarization ratios). The 0° and 90° directions are established using the incident collimated LB and the incident beam after deflection by a pentaprism. The axis of the focused LB (NA=0.09, 10° angular diameter) (NA denotes numerical aperture) was aligned to the 0° direction within 0.1° by centering the laser focus lens on the incident beam to within 0.03 mm, using a four-quadrant detector placed after the sample cell to detect beam displacement. The focused beam axis fluctuates around the 0° direction by about 0.1° due to beam pointing jitter of the laser.

The axis of the collection optics was aligned using the beam obtained by sending $\lambda=532$ nm light in the reverse direction through the collection optics assembly. With light injected from an 8 μm core diameter fiber at the H port and a 0.17 mm diameter aperture A1 [see Fig. 2(a)], a reverse beam with 2.4° angular diameter is obtained and the collection axis can be aligned to within 0.1°. HRS measurements were performed using larger apertures A1, and the collection axis alignment was maintained to within 0.1° by centering all apertures on the lens axis to within 5 μm. The aperture A1 sets the collection NA, and HRS measurements were made with several apertures to allow extrapolation to NA=0. The apertures had nominal diameters 1.0, 1.5, 2.0, 3.0, and 4.0 mm, and the collection NA (0.127, 0.194, 0.253, 0.384, and 0.507) was determined from the measured aperture diameter and a ray trace of the optics. Except for the largest aperture, the collection NA agreed with the effective NA assessed photometrically using two photon fluorescence (2PF) or an integrating sphere light source. For the largest aperture the effective NA=0.47 was used in the analysis. The mean square slope of the laser wavefronts in the viewed volume with diameter 70 μm near the beam waist is 30× smaller than the mean square slope of the collected wavefront for the smallest (1.0 mm) collection aperture, and has been neglected. The largest aperture collected light over an angular diameter of 61°.

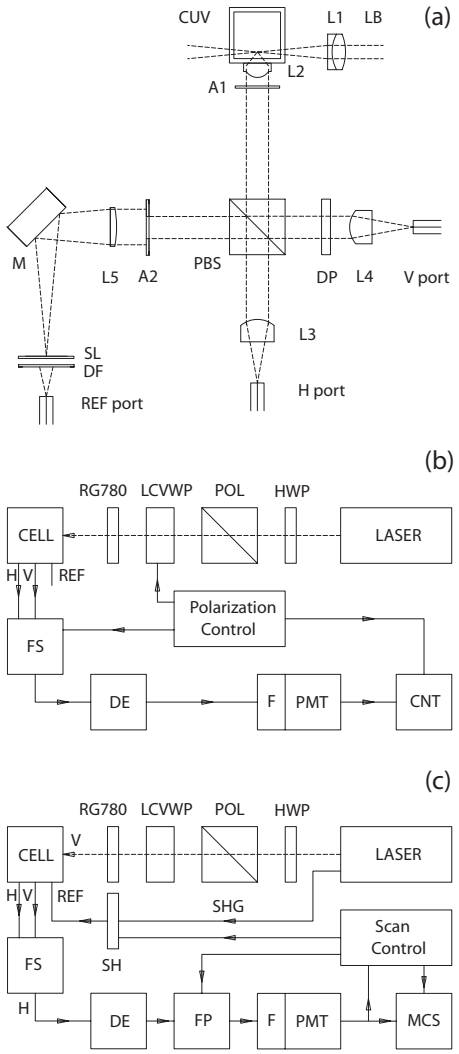

FIG. 2. HRS apparatus showing (a) top view of the sample and collection optics assembly and configurations for (b) polarization or (c) high resolution spectral measurements. (a) The laser beam (LB) is focused by lens L1 ($f=16$ mm) to an 8 μm diameter beam waist inside the 10 mm sample cuvette (CUV), and the scattered light is collected and collimated by aspheric lens L2 ($f=4.0$ mm), with NA set by aperture A1. H polarized light transmitted through the polarizing beam splitter (PBS) is focused by aspheric lens L3 ($f=11$ mm) into the output optical fiber at the H port, while the V polarized reflected light passes through a dichroic polarizer (DP) and is focused by aspheric lens L4 ($f=11$ mm) into the fiber at the V port. Light input from the fiber at the REF port passes through a diffuser (DF) and slit (SL), is collimated by the mirror (M), lens (L5) and aperture (A2), and the reference beam reflected by the PBS is focused into the output fiber at the H port. (b) The polarization and power of the beam from the laser is set by the half wave plate (HWP), prism polarizer (POL) and LCVWP, and any visible light is removed by the RG780 filter before reaching the sample and collection optics assembly (CELL). The fiber switch (FS) selects light from either the H or V port, which is spectrally filtered by a dual étalon (DE, 0.3 cm^{-1} FWHM) and interference filter (F, 60 cm^{-1} FWHM), then detected and recorded by a photomultiplier tube (PMT) and counters (CNT). Signals from the controller switch the LCVWP and FS, and gate the counters. (c) HRS spectral measurements use a scanning confocal FP inserted before the PMT and a multichannel scaler (MCS) counting the PMT pulses. The scan controller stabilizes the FP scans using the reference signal produced by intermittently passing second harmonic light from the laser (SHG) through the shutter (SH) to the REF port.

The collection optics and cuvette holder (but not the laser focus lens) were parts of a single assembly that was rotated or translated as a unit to adjust the scattering angle and place the LB waist at the focus of the collection optics. The

focus is located 5 mm from the entrance window of the 10 mm cuvette, and is 1.6 mm behind the viewing window. The mean scattering angle was restricted to a small range near 90° to prevent obstruction of the LB by a corner of the rotated cuvette. The collected HRS light is divided by the polarizing beam splitter (PBS) into two beams that are coupled to separate 200 μm optical fibers (the images of the HRS source are simultaneously centered on the fiber cores). The poor polarization purity of the reflected beam from the PBS was corrected by inserting a dichroic polarizer (DP) in that beam, so the extinction ratio was better than 5×10^{-4} for both output ports of the polarization analyzer. The two output fibers were connected to an optical switch which coupled light from one or the other fiber into a third fiber leading to the remaining optics and the detector. This arrangement allowed observations to switch rapidly (<0.1 s) between V and H polarization for the HRS light. Since the polarization of the light propagating in the multimode fibers is not preserved but is also not scrambled it is important to make the fiber-coupled components polarization insensitive to avoid errors and erratic changes in calibration. To eliminate the effect of laser power fluctuations and drift, a typical experimental polarization ratio measurement consisted of HRS photon counts recorded for two different polarization configurations while alternating between the two configurations at 10 s intervals for several hundred cycles. Spectral analysis was performed by an interference filter just before the detector to select a band centered at 532 nm with bandwidth $\Delta\nu=60$ cm^{-1} [full width at half maximum (FWHM)], and a fiber-coupled, dual-étalon filter that could be inserted to narrow the selected spectral band to 0.3 cm^{-1} (the average transmission of this filter outside the nominal passband was 6% of the peak transmission). Higher spectral resolution (13 MHz) was obtained by inserting a fiber-coupled, scanning confocal Fabry–Pérot (FP) interferometer as previously described.[15]

The accuracy of the polarization ratio measurements depends on several calibrations and corrections. The LB was prepared with V polarization by a Glan-laser prism polarizer, followed by an electronically controlled liquid crystal variable wave plate (LCVWP) to switch between V and H polarization for the LB to the sample. The measured transmission of the LCVWP was 0.1% lower for H versus V transmitted polarization (due to larger liquid crystal director fluctuations at low applied voltage). The HRS scattering angle is changed by rotating the cuvette and the reflection at the entrance face becomes polarization dependent as the cuvette is rotated away from normal incidence. The analysis accounts for the polarization dependence of the LB power in the sample due to these effects.

The polarization dependence for collection and detection of the HRS light was calibrated by substituting and measuring an unpolarized source. Thus, the relative collection, transmission and detection efficiency for V versus H polarized light (η_V/η_H) was calibrated at each NA by measuring I_{HV}/I_{HH} for 2PF from 0.5 mM disodium fluorescein dissolved in D_2O. Rhodamine 6G has previously been used for such calibration,[11] and its 2PF cross section is 100× larger than that of fluorescein,[20] but in the present experiment deviations from unpolarized emission up to 3% were observed with rhodamine 6G even though HV and HH should be equivalent by symmetry. These deviations were largest at high laser power and low dye concentration. Fluorescein is better since the 2PF emitted at 532 nm for fluorescein is from the lowest vibrational level of the excited electronic state, whereas for rhodamine 6G this light is emitted from vibrationally excited molecules before they relax to the vibrational ground state, allowing too little time for complete orientation relaxation. An alternative calibration using light from an incandescent lamp fiber-coupled into an integrating sphere at the sample position gives results similar to 2PF, but not identical. The calibration differences result from the different spatial distributions for these two light sources. The 2PF source image is a thin band across the fiber core and the calibration is sensitive to mismatch between the 2PF image positions on the H and V fibers, whereas this has no effect for the integrating sphere source since it uniformly floods both fibers with light. However, the integrating sphere result is more sensitive to differences in fiber core diameter. The calibration uses 2PF since the HRS and 2PF sources have nearly the same spatial distribution. The η_V/η_H calibration was found to be NA dependent, which can result from the less sharp imaging at large NA reducing the effect of image position mismatch and increasing the effect of different fiber diameter. Image blur can also account for the reduced effective NA for the largest aperture. As a result of imperfect control of such effects, the stability of the calibration was not as good as the 0.1% uncertainty of the η_V/η_H measurements.

The refractive index of the sample is needed to determine ray directions inside the sample; the mean scattering angle θ is given by $\theta=90°+\Delta\theta$, where $\Delta\theta=\arcsin(\sin(\Delta\theta')/n_{1064})\approx\Delta\theta'/n_{1064}$ and $\Delta\theta'$ is the sample cell rotation angle. The value $n_{532}=1.55$ at $\lambda=532$ nm and $T=25.0$ °C has been taken for $C_6D_5NO_2$ based on the reported measurements for nitrobenzene at visible wavelengths.[21,22] Since there are no refractive index measurements for nitrobenzene at $\lambda=1064$ nm, n_{1064} was measured for $C_6D_5NO_2$ *in situ*, by rotating the cuvette and observing the motion of the étalon fringes across the collimated LB reflected from the cuvette.[23] The result is $n_{1064}=1.43\pm0.03$, which disagrees with an extrapolation of the nitrobenzene values in the visible but agrees with the extrapolation of results inferred from a stimulated Raman experiment which show a sharp downturn in the dispersion curve starting at about $\lambda=850$ nm.[24]

IV. RESULTS AND DISCUSSION

The results of these experiments are the three HRS intensity ratios I_{VV}/I_{HV}, I_{HV}/I_{VH}, and I_{HH}/I_{VH} measured as functions of scattering angle over the range of $90°\pm3.5°$. However, even the smallest aperture employed in the measurements collects HRS light over a 9° angular diameter in the sample, which is larger than the range for the mean scattering angle. The effect of averaging the polarization ratios over such large collection apertures is dealt with empirically by fitting a quadratic polynomial in NA^2 to the measurements and extrapolating to NA=0, as shown in Fig. 3.

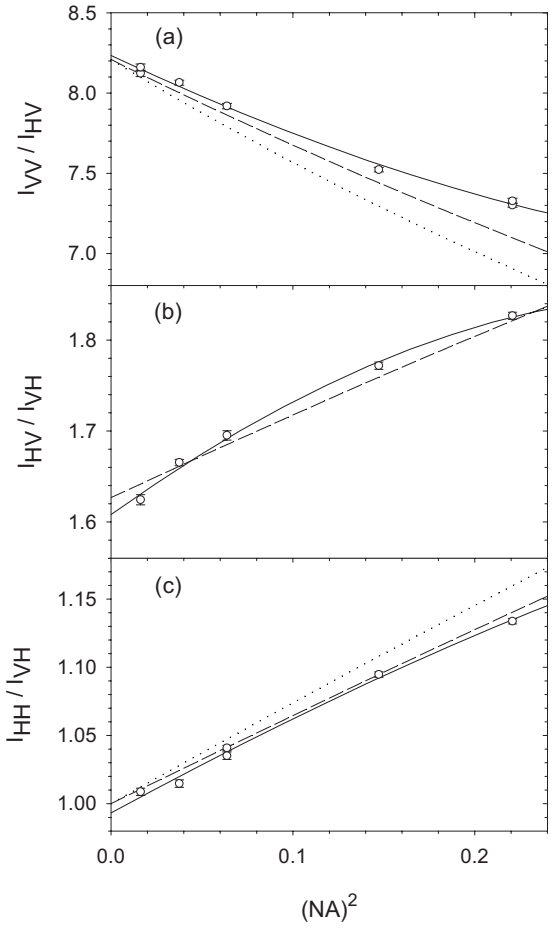

FIG. 3. Extrapolation to NA=0 for typical measurements of the HRS polarization ratios (a) $I_{VV/HV}$, (b) $I_{HV/VH}$, and (c) $I_{HH/VH}$ for $C_6D_5NO_2$. The open circles are data for $\Delta\theta=0°$ and $\Delta\nu=0.3$ cm^{-1} with error bars showing the uncertainties due to photon counting statistics. The solid curves are the fitted polynomials used to extrapolate the data, while the dashed curves were calculated using the parameters from Table II. The dotted curves are calculated assuming pure local mode HRS with $P^2=8.21$.

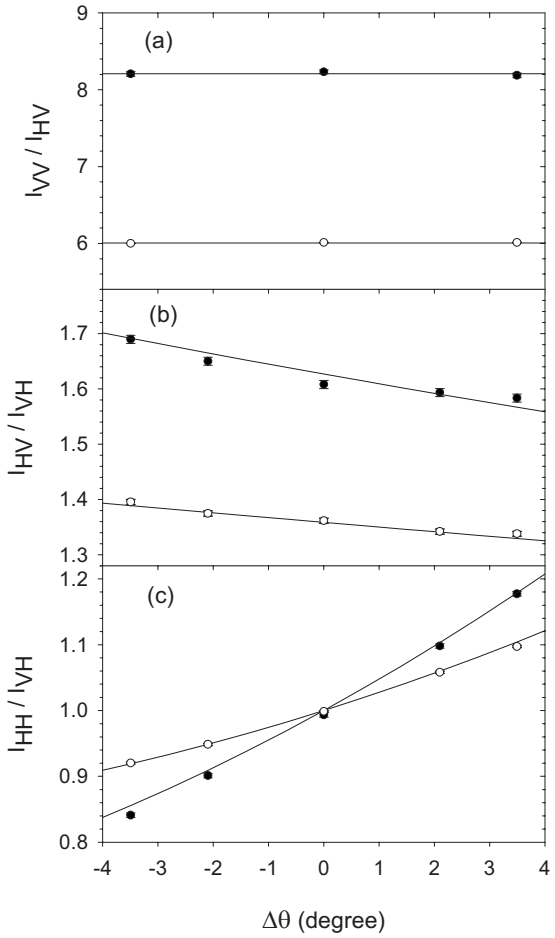

FIG. 4. Experimental results for the HRS polarization ratios (a) $I_{VV/HV}$, (b) $I_{HV/VH}$, and (c) $I_{HH/VH}$ at NA=0 for $\Delta\nu=0.3$ cm^{-1} (filled circles) and $\Delta\nu=60$ cm^{-1} (open circles) are plotted vs the change in scattering angle $\Delta\theta=\theta-90°$. The solid curves are the fit of Eqs. (1)–(4) to the data with the parameters from Table II.

Theory suggests this truncated power series and predicts that the NA^4 term will be small for the angular apertures used in the measurements. The results of these extrapolations are shown in Table I and Fig. 4. Polarization ratios were measured with a spectral bandwidth $\Delta\nu=0.3$ cm^{-1} to select just the central peak of the HRS spectrum for nitrobenzene, and with $\Delta\nu=60$ cm^{-1} to give the integrated intensity of the entire spectrum. The longitudinal mode contribution due to dissolved ions was assessed by scanning the VH spectrum with 13 MHz resolution. The high resolution VH HRS spectrum consists of a narrow unresolved spike riding on a broad, flat background, where the spike is the longitudinal mode contribution induced by the ions.[14] The measured ratio of integrated intensities for the spike and the background was $S/B=0.0223\pm0.0016$ for $\Delta\nu=0.3$ cm^{-1} and 0.0061 ± 0.0008 for $\Delta\nu=60$ cm^{-1} (ion concentration about 0.5 μM based on Ref. 15).

TABLE I. HRS polarization ratios for $C_6D_5NO_2$ vs cell rotation angle $\Delta\theta'$ at NA=0 for $\Delta\nu=0.3$ or 60 cm^{-1} spectral bandwidth. The error bars represent the uncertainty of extrapolation to NA=0, as shown in Fig. 3.

$\Delta\nu$ (cm^{-1})	$\Delta\theta'$ (deg)	I_{VV}/I_{HV}	I_{HV}/I_{VH}	I_{HH}/I_{VH}
0.3	−5	8.21 ± 0.03	1.690 ± 0.007	0.841 ± 0.003
0.3	−3	⋯	1.650 ± 0.007	0.901 ± 0.003
0.3	0	8.23 ± 0.03	1.608 ± 0.007	0.993 ± 0.003
0.3	3	⋯	1.594 ± 0.007	1.098 ± 0.003
0.3	5	8.19 ± 0.03	1.584 ± 0.007	1.177 ± 0.003
60	−5	6.00 ± 0.02	1.396 ± 0.005	0.920 ± 0.002
60	−3	⋯	1.375 ± 0.005	0.949 ± 0.002
60	0	6.01 ± 0.02	1.362 ± 0.005	0.999 ± 0.001
60	3	⋯	1.342 ± 0.005	1.058 ± 0.002
60	5	6.01 ± 0.02	1.338 ± 0.004	1.097 ± 0.002

The results of this experiment may be compared to several previous measurements for nitrobenzene.[9,11] The results from Ref. 9 are $I_{VV}/I_{VH}=7.6\pm0.2$ and $I_{HV}/I_{VH}=1.08\pm0.01$, measured with $\Delta\nu=25$ cm^{-1} and with a calculated correction applied for the finite collection aperture. Combining these results gives $I_{VV}/I_{HV}=7.0$ which falls midway between the results in Table I for $\Delta\nu=0.3$ and 60 cm^{-1} spectral bandwidth. The result for I_{HV}/I_{VH} disagrees with the present results, but can be explained by ionic contamination of the previous sample. The results for I_{VV}/I_{VH} and I_{HV}/I_{HH} in Ref. 11 apparently were not corrected for the NA=0.34 collection aperture. They are in qualitative agreement with the present results, decreasing as the bandwidth increases in

TABLE II. Parameter values for the fit of Eqs. (1)–(4) to the data in Table I.

Parameter	$\Delta\nu$=0.3 cm^{-1}	$\Delta\nu$=60 cm^{-1}
P^2	1.5	1.5
R	3.114 ± 0.043	3.114 ± 0.043
A_0/A_T	0.221 ± 0.041	0.818 ± 0.060
A_L/A_T	0.059 ± 0.030	0.030 ± 0.029
$(A_L/A_T)_{\min}$	0.035 ± 0.003	0.017 ± 0.002

the range $\Delta\nu$=4–64 cm^{-1}, but the results I_{VV}/I_{VH}=6.5 and I_{HV}/I_{HH}=1.30 ± 0.06 at $\Delta\nu$=64 cm^{-1} are lower than the corresponding values 8.2 and 1.36 at similar NA and $\Delta\nu$ obtained from the present experiment. Overall, there is rough agreement between the results of the previous and present experiments.

The polarization ratio data in Table I and Fig. 4 were fit using expressions for the HRS intensity ratios I_{VV}/I_{HV}, I_{HV}/I_{VH}, and I_{HH}/I_{VH} constructed using Eqs. (1)–(4). The fit results are shown in Table II and Fig. 4. The P^2 and R parameter values were required to be the same for the fits to the $\Delta\nu$=0.3 and $\Delta\nu$=60 cm^{-1} data sets, but the A_0/A_T and A_L/A_T parameter values were different for the two data sets. Minimum values for A_L/A_T imposed as constraints on the fits are shown in the last line of Table II. This constraint accounts for the longitudinal mode contribution due to ions, which is directly measured by the VH spike. The value P^2=1.5 has also been imposed on the fits shown in Table II and Fig. 4. The best fit with P^2 free to vary gave the unphysical value P^2=0.2, and while values as large as 3.6 are rejected by the fit, all values $P^2 \leq 1.5$ give insignificantly different fit results. The value P^2=1.5 is consistent with the data and is suggested by a theoretical argument (see below). The fit functions shown in Fig. 4 are able to account for the main features of the data, but for some of the points the difference between the fit function and the data is larger than the error bars.

Another comparison between the theoretical model and the observations is presented in Fig. 3, where calculated HRS polarization ratios as functions of NA for the collection optics are shown by the dashed curves. The calculation of the HRS intensities averaged over the collection aperture uses the parameters in Table II, and includes scattering angles out of the horizontal plane using Eqs. (3)–(6) and (14)–(17) of Ref. 12 and Eqs. (A4)–(A7) in the Appendix (for the angular dependence of the HRS intensity). Additional factors included in the calculation are the depolarization due to skew reflection at the cuvette exit face and due to collimation of the scattered light.[25] Let ϕ, ψ be the angles in the horizontal plane and the out-of-plane directions, respectively, measured from the collection optic axis which is also the normal to the cuvette exit face. The ray in this direction is incident on the cuvette face at angle β=arccos(cos ϕ cos ψ) with intensity transmission ratio $T_\perp(\beta)/T_\parallel(\beta)$ for the components polarized perpendicular and parallel to the plane of incidence. Collimation of this ray also rotates the electric field vector in the plane of incidence but not the perpendicular vector. The net effect of Fresnel reflection and collimation is to rotate the linear polarization of the incident ray by an angle α =arctan$[(T_\perp/T_\parallel)^{1/2}\sin\phi \sin\psi/(\cos\phi+\cos\psi)]$. The maximum rotation is $<2°$ at the edge of the largest aperture, and the effect on the HRS polarization ratios averaged over the aperture is small. Other aperture-dependent polarization discrimination effects acting after the polarizer are measured and accounted for in the instrument calibration function.

Figure 3 shows discrepancies between the results of this calculation and the measurements. Although the discrepancies are larger than the uncertainties due to photon counting statistics (the plotted error bars), they are not much larger than the uncertainties due to uncontrolled variations in the alignment and calibration of the apparatus (the largest calibration uncertainties are associated with the I_{HV}/I_{VH} measurements). The discrepancies are much larger for the results calculated assuming pure local mode HRS, also plotted in Fig. 3 for comparison. The largest differences between the data and the calculated curves tend to occur at large NA, which indicates that applying calculated corrections for finite aperture effects[7] to HRS measurements at large NA is less reliable than extrapolation of a series of measurements to NA=0.[26]

The pure local mode curves in Fig. 3 were calculated assuming only dipole hyperpolarizability contributions, and one may consider whether agreement with the I_{HV}/I_{VH} observations can be obtained by including quadrupolar and magnetic HRS contributions. These contributions for spherical molecules[18,19] and nanoparticles[27] are $I_{VV}=I_{HV}=|\kappa_1 \sin\theta \sin 2\psi|^2$, $I_{VH}=|\kappa_1 \sin 2\theta \sin^2\psi+(\kappa_2+\kappa_3)\sin\theta|^2$, and $I_{HH}=|\kappa_1 \sin 2\theta \cos^2\psi+(\kappa_2+\kappa_3)\sin\theta|^2$, where κ_1, κ_2, and κ_3 are the amplitudes for the qee, eeq, and eem contributions, the mee contribution vanishes, and $|\kappa_1/\kappa_2|=1$ for spherical molecules. Simply assuming the same form for the nonspherical nitrobenzene molecule and adding these contributions to the β dipole hyperpolarizability (eee) contribution decreases I_{HV}/I_{VH} (the wrong direction) and leaves I_{VV}/I_{HV} and I_{HH}/I_{VH} unchanged (at θ=90° and ψ=0°). The intensities add since the tensors for the additional contributions have parity opposite to the β tensor, so that interference terms vanish when averaged over molecular orientations. The values of these hyperpolarizability tensors for nitrobenzene are presently unknown, but if they are only as large as the corresponding tensors for benzene[28] their HRS intensity contribution would be about 10^{-5} times the β contribution, which is negligibly small.

Thus, the data shown in Fig. 4 are inconsistent with pure local mode HRS and are in fair agreement with the mixed local and collective mode model expressed by Eqs. (1)–(4). The fit parameters in Table II may be interpreted as follows. The value R=3.114 is consistent with HRS from polar collective modes with a small deviation from Kleinman symmetry, while the value P^2=1.5 is consistent with incoherent scattering from the octupolar term $\beta^{(3)}$. Polar collective mode HRS is due to orientation correlations acting to give coherent scattering over an extended volume for the vector term $\beta^{(1)}$, but these correlations cannot result in coherent scattering for the octupolar term $\beta^{(3)}$. It is not necessary to include a separate incoherent contribution for the vector term $\beta^{(1)}$ since an arbitrary vector distribution can be represented by an appropriate superposition of transverse and longitudi-

nal modes. In the case that the transverse and longitudinal mode intensities are equal the result would be indistinguishable from incoherent scattering from the vector term $\beta^{(1)}$, where $R^2=9.7$ instead of 9 again indicates a deviation from Kleinman symmetry. From the fit parameter difference $(A_L/A_T)-(A_L/A_T)_{\min}$ in Table II one sees that the longitudinal mode contribution to HRS for pure nitrobenzene is small, less than 2% of I_{VH}. From the fit parameters P^2, R, and A_0/A_T one sees that the transverse mode contribution is 82% of I_{HV} and 97% of I_{VV} for the central peak of the spectrum, while for the entire spectrum the contributions are 55% and 89%, respectively. The transverse collective mode contribution dominates the HRS peak for nitrobenzene while the octupolar contribution is more prominent in the wings of the spectrum, but the observed octupolar contribution is only about half that predicted from the static *ab initio* β assuming incoherent HRS.[16]

The vector part of β transforms just like the dipole moment of a polar molecule, so the near zero contribution of the longitudinal mode to the HRS peak can be understood by considering the dielectric properties of a dense fluid of nonpolarizable dipolar molecules with number density ρ and dipole moment μ.[29] The pair distribution function for the dipolar molecules can be expressed as the sum of a function (g^{S}=Kirkwood factor g^K) including short range orientation correlations extending only a few molecular diameters, and a function (g^{L}) including only the long range correlations due to dipole-dipole interactions. For $k\rightarrow 0$, large static permittivity $\varepsilon(0)$, and $g^{\mathrm{S}}=1$, the mean square transverse and longitudinal Fourier components of the sample dipole moment density are $\langle|M_X(\mathbf{k})|^2\rangle=\frac{1}{2}\rho\mu^2$ and $\langle|M_Z(\mathbf{k})|^2\rangle=\frac{1}{2}\rho\mu^2/\varepsilon(0)$, and in the rotational diffusion limit the transverse and longitudinal relaxation times are τ_D and $\tau_D/\varepsilon(0)$, respectively, where τ_D is the Debye relaxation time.[29] The dipoles in the liquid are arranged as large amplitude transverse modes and small amplitude longitudinal modes due to the long range dipole-dipole interactions, and the temporal fluctuations result in a narrow spectral peak for the transverse modes and a much broader peak for the longitudinal modes. The asymmetry between transverse and longitudinal mode properties scales as the static permittivity $\varepsilon(0)$, which has the value $\varepsilon(0)=35$ for nitrobenzene.[30] This picture should be at least qualitatively correct for real liquid nitrobenzene with polarizable molecules and $g^K=1.56$.[31]

V. SUMMARY

The observed polarization dependence of HRS from liquid nitrobenzene is not consistent with randomly oriented molecules or molecules with only local orientation correlations. A model for polar collective mode contributions to HRS is presented and shown to agree with the main observations, although there appear to be small quantitative discrepancies between the model predictions and the experimental observations. Two of the observed effects of transverse polar mode contributions to HRS that are inconsistent with local modes are: $I_{\mathrm{HV}}>I_{\mathrm{VH}}$ and $(\partial I_{\mathrm{HH}}/\partial\theta)>0$ at $\theta=90°$, although care is required to prevent the effects of large collection aperture or ionic contamination from masking or confusing these observations. The picture supported by the HRS observations is that dipole-dipole interactions in polar liquids result in long range transverse orientation correlations of the molecules which are impressed on HRS from the vector term $\beta^{(1)}$ but do not affect HRS from the octupolar term $\beta^{(3)}$.

APPENDIX: ANGULAR DEPENDENCE FOR TRANSVERSE MODE HRS

Equations (10)–(13) of Ref. 12 for transverse mode HRS are incorrect, and the correct expressions are given below. The error arises in Eq. (8) of Ref. 12 for one of the mutually orthogonal basis vectors $\hat{\mathbf{K}}$, $\hat{\mathbf{Q}}_{T1}$, and $\hat{\mathbf{Q}}_{T2}$ specifying the direction and polarization of the transverse polar modes. The vectors are expressed using the coordinate system in Fig. 1, where the incident wavevector $\mathbf{k}_\nu$ is along Y, the incident polarization is either along Z or X (V or H, respectively), and the scattered wavevector $\mathbf{k}_{2\nu}$ is in direction $\hat{\mathbf{R}}=\lambda_X\hat{\mathbf{X}}+\lambda_Y\hat{\mathbf{Y}}+\lambda_Z\hat{\mathbf{Z}}$ specified by the direction cosines $\lambda_X=\hat{\mathbf{R}}\cdot\hat{\mathbf{X}}=\sin\theta\cos\psi$, $\lambda_Y=\cos\theta\cos\psi$, and $\lambda_Z=\sin\psi$. The angle θ is measured from the Y axis in the XY plane, and ψ is the angle above the XY plane. The unit vector $\hat{\mathbf{K}}$ is in the direction of scattering vector $\Delta\mathbf{k}=2\mathbf{k}_\nu-\mathbf{k}_{2\nu}$, the unit vector $\hat{\mathbf{Q}}_{T1}$ is chosen perpendicular to $\hat{\mathbf{Z}}$, and $\hat{\mathbf{Q}}_{T2}=-\hat{\mathbf{K}}\times\hat{\mathbf{Q}}_{T1}$.

$$\hat{\mathbf{K}}=\frac{(1-\lambda_Y)\hat{\mathbf{Y}}-\lambda_X\hat{\mathbf{X}}-\lambda_Z\hat{\mathbf{Z}}}{[2(1-\lambda_Y)]^{1/2}}, \tag{A1}$$

$$\hat{\mathbf{Q}}_{T1}=\frac{\lambda_X\hat{\mathbf{Y}}+(1-\lambda_Y)\hat{\mathbf{X}}}{[(1-\lambda_Y)^2+\lambda_X^2]^{1/2}}, \tag{A2}$$

$$\hat{\mathbf{Q}}_{T2}=\frac{(1-\lambda_Y)\lambda_Z\hat{\mathbf{Y}}-\lambda_X\lambda_Z\hat{\mathbf{X}}+[(1-\lambda_Y)^2+\lambda_X^2]\hat{\mathbf{Z}}}{[(1-\lambda_Y)^2+\lambda_X^2]^{1/2}[2(1-\lambda_Y)]^{1/2}}. \tag{A3}$$

Equation (A3) corrects the error in Eq. (8) of Ref. 12, and Eq. (A2) corrects the misprint in Eq. (7) of Ref. 12. Proceeding as in Ref. 12, one obtains the following expressions for the transverse mode HRS intensities:

$$I_{\mathrm{VV}}/A_T=\frac{\sin^2\theta\sin^2\psi}{1+\cos^2\psi-2\cos\theta\cos\psi}+\frac{[(\cos\psi-\cos\theta)\sin^2\psi+R\cos\psi(1+\cos^2\psi-2\cos\theta\cos\psi)]^2}{2(1-\cos\theta\cos\psi)(1+\cos^2\psi-2\cos\theta\cos\psi)}, \tag{A4}$$

$$I_{HV}/A_T = \frac{[1+(R-1)(1-\cos\theta\cos\psi)]^2\sin^2\theta\sin^2\psi}{1+\cos^2\psi-2\cos\theta\cos\psi} + \frac{[(\cos\psi-\cos\theta+(R-1)\sin^2\theta\cos\psi)\sin^2\psi+\cos\psi(1+\cos^2\psi-2\cos\theta\cos\psi)]^2}{2(1-\cos\theta\cos\psi)(1+\cos^2\psi-2\cos\theta\cos\psi)}, \tag{A5}$$

$$I_{VH}/A_T = \frac{[\cos\psi-\cos\theta]^2}{1+\cos^2\psi-2\cos\theta\cos\psi} + \frac{\sin^2\theta\sin^2\psi}{2(1-\cos\theta\cos\psi)(1+\cos^2\psi-2\cos\theta\cos\psi)}, \tag{A6}$$

$$I_{HH}/A_T = \frac{[\cos\psi-\cos\theta-(R-1)\cos\theta(1-\cos\theta\cos\psi)]^2}{1+\cos^2\psi-2\cos\theta\cos\psi} + \frac{[1+(R-1)\cos\theta\cos\psi]^2\sin^2\theta\sin^2\psi}{2(1-\cos\theta\cos\psi)(1+\cos^2\psi-2\cos\theta\cos\psi)}. \tag{A7}$$

The HRS intensities for the two special cases with $\{A_0=1,\ A_T=A_L=0\}$ or $\{A_0=0,\ A_T=A_L=1\}$ are identical when $P^2=R^2$. This holds for each polarization and at all angles, and provides an error check for the above expressions.

[1] R. Bersohn, Y. H. Pao, and H. L. Frisch, J. Chem. Phys. **45**, 3184 (1966).
[2] P. D. Maker, Phys. Rev. A **1**, 923 (1970).
[3] M. Kauranen and A. Persoons, J. Chem. Phys. **104**, 3445 (1996).
[4] S. F. Hubbard, R. G. Petschek, K. D. Singer, N. D'Sidocky, C. Hudson, L. C. Chien, C. C. Henderson, and P. A. Cahill, J. Opt. Soc. Am. B **15**, 289 (1998).
[5] V. Ostroverkhov, R. G. Petschek, K. D. Singer, L. Sukhomlinova, R. J. Twieg, S.-X. Wang, and L. C. Chien, J. Opt. Soc. Am. B **17**, 1531 (2000).
[6] I. D. Morrison, R. G. Denning, W. M. Laidlaw, and M. A. Stammers, Rev. Sci. Instrum. **67**, 1445 (1996).
[7] P. Kaatz and D. P. Shelton, Rev. Sci. Instrum. **67**, 1438 (1996).
[8] P. Kaatz and D. P. Shelton, J. Chem. Phys. **105**, 3918 (1996).
[9] D. P. Shelton, Chem. Phys. Lett. **325**, 513 (2000).
[10] D. P. Shelton, J. Chem. Phys. **123**, 084502 (2005).
[11] J. Chen and K. Y. Wong, J. Chem. Phys. **122**, 174505 (2005).
[12] D. P. Shelton, J. Opt. Soc. Am. B **17**, 2032 (2000).
[13] V. N. Denisov, B. N. Mavrin, and V. B. Podobedov, Phys. Rep. **151**, 1 (1987).
[14] D. P. Shelton, J. Chem. Phys. **130**, 114501 (2009).
[15] D. P. Shelton, J. Chem. Phys. **129**, 134501 (2008).
[16] R. H. C. Janssen, D. N. Theodorou, S. Raptis, and M. G. Papadopoulos, J. Chem. Phys. **111**, 9711 (1999).
[17] S. Kielich, Phys. Lett. **27A**, 307 (1968).
[18] S. Kielich, M. Kozierowski, Z. Ozgo, and R. Zawodny, Acta Phys. Pol. A **A45**, 9 (1974).
[19] R. W. Munn, Z. Shuai, and J.-L. Bredas, J. Chem. Phys. **108**, 5975 (1998).
[20] P. Kaatz and D. P. Shelton, J. Opt. Soc. Am. B **16**, 998 (1999).
[21] J. Timmermans, *Physico-Chemical Constants of Pure Organic Compounds* (Elsevier, New York, 1950), Vol. 1.
[22] X. An, H. Zhao, F. Jiang, C. Mao, and W. Shen, J. Chem. Thermodyn. **29**, 1047 (1997).
[23] B. Šantić, D. Gracin, and K. Juraić, Appl. Opt. **48**, 4430 (2009).
[24] H. J. Zeiger, P. E. Tannenwald, S. Kern, and R. Herendeen, Phys. Rev. Lett. **11**, 419 (1963).
[25] M. Kauert, M. Frenz, and J. Ricka, Opt. Eng. **47**, 014201 (2008).
[26] S. W. Wong and K. Y. Wong, Opt. Commun. **133**, 268 (1997).
[27] J. I. Dadap, J. Shan, and T. F. Heinz, J. Opt. Soc. Am. B **21**, 1328 (2004).
[28] A. Rizzo, C. Cappelli, B. Jansik, D. Jonsson, P. Salek, S. Coriani, and H. Agren, J. Chem. Phys. **121**, 8814 (2004).
[29] P. Madden and D. Kivelson, Adv. Chem. Phys. **56**, 467 (1984).
[30] *CRC Handbook of Chemistry and Physics*, 68th ed., edited by R. C. Weast (CRC, Boca Raton, FL, 1987).
[31] L. Blum and R. W. Fawcett, J. Phys. Chem. **100**, 10423 (1996).